VISUAL ADAPTATION IN MOUSE PRIMARY VISUAL CORTEX

by

Jillian L. King

Submitted in partial fulfilment of the requirements
for the degree of Master of Science

at

Dalhousie University
Halifax, Nova Scotia
December 2014

DEDICATION PAGE

I would like to dedicate this thesis to my partner in crime, Austin Korgan. Austin has provided me with unlimited support throughout my unconventional MSc. During the data collection period he delivered suppers to the lab without fail, which is such a luxury when one is stuck at school until 4am regularly. During the data analysis and writing portion he gave me space, and throughout the entire process he always consoled me when I felt like I was never going to finish. Thank you, Austin. This degree would not have been possible without you.

TABLE OF CONTENTS

LIST OF FIGURES

ABSTRACT

Studying vision in mice is a relatively recent endeavor, with most research dating within the last 10 years. One goal of this research is to examine similarities and differences between the mouse visual system and more traditional animal models. This thesis contains two such studies, with the results from each suggesting that the mouse is a legitimate model for visual studies. The first study examines orientation adaptation and demonstrates that after orientation adaptation mouse orientation tuning curves shift similarly to what is observed in cats and primates. The second study looks at contrast adaptation, and provides evidence that it not spike rate dependent but rather pattern-specific. Combined, these studies suggest that mouse primary visual cortex adjusts to its visual surroundings comparably to traditional animal models, and also provide more of a foundation for future experiments utilizing genetic tools that are only available in mice.

LIST OF ABBREVIATIONS USED

cpd	Cycles per Degree
D.I.	Discrimination Index
dLGN	Dorsal Lateral Geniculate Nucleus
ISI	Interstimulus Interval
LGN	Lateral Geniculate Nucleus
RF	Receptive Field
RGCs	Retinal Ganglion Cells
SF	Spatial Frequency
SS	Surround Suppression
TF	Temporal Frequency
TTL	Triggered Transistor-Transistor Logic
V1	Primary Visual Cortex

ACKNOWLEDGEMENTS

I have a lot of amazing people to thank for all of their help and support in making this MSc a reality. First of all, I would like to thank my supervisor Dr. Nathan Crowder for taking a chance on me two and a half years ago. Nathan has provided endless support and motivation, and has been a fantastic mentor. His door is always open, and he put everything he had into making my MSc the best it could be. Thank you for all the time you have invested into my just-beginning academic career, I am excited to see how much better my PhD will be! Next, I would like to thank the best summer student ever, Matt Lowe, for all of his help with data collection and analysis. You're a star in the making, Ice. I would also like to thank my committee, Drs. Donald Mitchell and Dennis Phillips, and the other member of the Vision group, Dr. Kevin Duffy, for their support and advice during committee meetings and whenever I just needed a chat. Finally, I would like to thank my family - Mom, Dad, Patrick and Paddy and Sharon - for their love and patience in what has been a drawn out and sometimes-frustrating experience. It's finished!

CHAPTER 1: INTRODUCTION

1.1 Animal Models of Human Visual Cortical Processing

Organisms' abilities to navigate their environments come from sensory systems: audition, gustation, somatosensation, olfaction and vision. Vision is the ability to interpret light information. Humans are highly visual creatures, and it is perhaps for this reason that vision is the most studied sense.

In an attempt to determine the underlying neural circuitry and molecular processes that regulate visual perception, as well as manufacture and improve treatments for visual deficits, researchers make use of animal models. In the past, visual perception research primarily focused on non-invasive psychophysical techniques, but over the past 75 years (from Hartline, 1934) attention has shifted to more invasive immunohistological and neurophysiological studies which cannot be performed in humans. These studies utilizing animal models have started to undercover the neural mechanisms responsible for visual processing, and have begun to establish causal links between perception and neural circuits.

Cats and primates are extremely visual animals, and have been used as the animal model for many of the experiments that have set the foundation for visual neuroscience (for example, Hubel & Wiesel, 1963). However, over the last 10 years mice have become an increasingly popular visual model (for commentary, see Baker, 2013). This introduction of mice to vision research after decades of work on cats and primates is a hotly debated topic, with many researchers believing that the mouse visual system is too simple for their findings to be relevant to humans. However, the genetic toolbox available

in mice is not yet readily accessible in any other mammalian animal model, and the opportunities presented by these tools are too great for vision researchers to dismiss.

Experimental possibilities with transgenic mice are endless. Specific cell types can be fluorescently labeled, up/down regulated, or even controlled via light by insertion of optogenetic molecules. Optogenetics has revolutionized neuroscience by allowing temporally accurate control of neural activity via light stimulation with precision that is pharmacologically unattainable. These molecular means have given researchers new opportunities, and for the first time causal links between neural machinery and perception can be explored. However, scientists are still unsure whether the findings obtained from mice are transferrable to more traditional models. As such, more baseline experiments need to be performed, and similarities to previous literature need to be more thoroughly evaluated.

1.2 Introduction to the Geniculate Pathway of Primate Models

Details regarding the primate visual system will be presented first as this is the "classic" system and has been more thoroughly studied. In Section 1.3 details of the mouse visual system will be described, and differences between the two systems will be discussed.

The fundamental components of the geniculostriate pathway are the eye, thalamic relay nuclei and visual cortical areas. Cats and monkeys, like humans, have forward facing eyes which can move easily (Fuchs et al., 1985; Schall et al., 1995). After light has entered the eye, it is processed by the retina. The retina contains two types of light-sensitive cells: rods and cones. There are more rods than cones, but in the primate retina

cones are concentrated in a central area known as the fovea, with an average peak density of ~210,000/mm^2 (Packer et al., 1989). Functionally, cones are responsible for high acuity vision and colour discrimination, whereas rods are responsible for seeing in dim light (Wikler and Rakic, 1990). Information from the photoreceptors is further processed by the retinal circuitry, and then exits the back of the eye through the axons of retinal ganglion cells (RGCs) which combine to form the optic nerve.

1.2.1 Organization and Function of the Lateral Geniculate Nucleus

RGCs project via the optic nerve to the lateral geniculate nucleus (LGN) of the thalamus, dividing at the optic chiasm such that half of the projections from each retina go to each hemisphere; projections from the nasal retina project to the contralateral hemisphere, and projections from the temporal retina project to the ipsilateral hemisphere. The LGN is responsible for regulating and organizing information flow from the retina to V1 (Irvin et al., 1993; Wimbauer et al., 1997). The LGN receives input from roughly 90% of retinal projections go to the LGN, as well as from the cortex and other LGN neurons. The LGN is organized into six layers. Layers 1, 4 and 6 receive input from the contralateral eye, and layers 2, 3 and 5 from the ipsilateral eye, with 6 being the most dorsal and 1 the most ventral. In addition to the layers being organized based on ocular input, they are also organized based on cell size. The more ventral layers of LGN, layers 1 and 2, are composed of larger cells known as the magnocellular layers, whereas the dorsal layers, 3-6, are composed of smaller cells and are known as the parvocellular layers. Finally, the LGN is also retinotopically organized, which means that neighbouring

RGCs send their input to neighbouring LGN neurons. The receptive fields (RF) of LGN neurons are also identical to that of RGCs: circular with an antagonistic surround.

1.2.2 Organization of the Primary Visual Cortex

The pathways from the LGN to the primary visual cortex (V1) in the occipital lobe of the brain are known as the optic radiation. Like the LGN, V1 is also organized into 6 layers: VI, V, IV, III, II and I, with VI being next to white matter and I next to the pial surface. Layers II/III are known as the supragranular layers, and V/VI are the intragranular layers. Layer IV is further subdivided into IVA, IVB, IVCα and IVCβ, which are collectively known as the granular layers (Callaway, 1998). Most of the input from LGN projects to layer IVC, with cells from the magnocellular layer connecting with neurons in IVCα and neurons from the parvocellular layer to IVCβ. V1 is also known as the striate cortex, which refers to the dense strip of myelinated axons which run parallel to the surface of the cortex in layer IV. Anatomically, within V1 there are two primary cell types, spiny stellate cells and pyramidal cells. Spiny stellate cells are located only within layer IVCβ and exclusively form local connections. Pyramidal neurons are located in all other layers, and are the output cells of V1.

1.3 Mouse Visual Pathway

This section will briefly cover the mouse visual pathway until V1, describing similarities and differences with the visual pathway of cats and primates. Mice have laterally positioned eyes which grant them only 30° of binocular overlap (Dräger, 1975a). These animals have both rods and cones, but lack a fovea as only 3% of their

photoreceptor population are cones (Porciatti et al., 1999). However, there is a slight increase in cone density in an area centralis (12,400/mm^2, Jeon et al., 1998). The retinal circuitry and projections in mice follow the typical mammalian scheme (Jeon et al., 1998), and once light information is processed by these cells it leaves the eye via the optic nerve. The projections from the retina also innervate similar regions to that of the primate, such as the superior colliculus and the LGN (Dräger and Olsen, 1980), and the LGN then projects to V1 (Rodieck and Watanabe, 1993). Mouse V1 is also strikingly similar to primates: it has 6 layers which receive retinotopically organized signals to create a visual representation of their surroundings (Schuett et al., 2002; Kalatsky and Stryker, 2003), and the LGN projects primarily to layer IV (Wang and Burkhalter, 2007).

Mouse vision is substantially less acute than higher-order mammals (their spatial and temporal acuity is roughly 100 and 5 times lower, respectively, than humans': Prusky, West, & Douglas, 2000), but baseline studies have shown that overall their visual system is functionally similarly to that of cats and monkeys (Gao, DeAngelis, & Burkhalter, 2010; Huberman & Niell, 2011; Marshel, Garrett, Nauhaus, & Callaway, 2011; Niell & Stryker, 2008; Wang & Burkhalter, 2007; for review see Huberman and Niell, 2011). It has been shown that mice exhibit both optokinetic nystagmus and optomotor behaviours (Balkema et al., 1984; Prusky et al., 2004), and that they are capable of performing visually guided water maze tasks (Prusky et al., 2000) and forced choice touchscreen tasks (Bussey et al., 2001; Busse et al., 2011).

1.4 Physiology of V1

Though the visual system of cats/primates and mice have many similarities, there are differences due to the laterally placed eyes and dichromatic vision in mice. As such, the next section will focus on properties of visual stimulus selectivity which are common between these species: orientation selectivity and spatial and temporal frequency tuning.

1.4.1 Orientation Selectivity

Outside of layer IVC in V1 there are no center-surround RFs as there are for RGCs and LGN neurons. Early descriptions of the RFs of V1 neurons generally have elongated, rectangular RFs which make them especially sensitive to the orientation of the stimulus (Hubel and Wiesel, 1968).A neuron will fire maximally to a stimulus which is oriented identically to its RF, and will fire progressively less as the stimulus angle gets further from the preferred. Some cells are also direction selective and will only respond to stimuli which are moving in one direction.

Physiologically, there are two principle classifications of cells in V1: simple cells and complex cells. Hubel and Wiesel (1962) were the first to describe these cells, and they were later classified in mouse (Niell & Stryker, 2008). The circuitry underlying simple and complex cells is still unclear, but it appears that simple cells are created by a linear summation of multiple center surround LGN inputs, with the ON and OFF subregions spatially separate (Reid and Alonso, 1995). ON subregions respond to bars of light and are inhibited by dark bars, whereas OFF subregions respond to dark bars and are inhibited by light bars. The receptive fields of complex cells do not have this organization as ON and OFF regions are not spatially segregated, and due to these differences the responses of simple and complex neurons to grating stimuli are distinguishable. Simple

cells are sensitive to the phase of a stimulus, responding maximally when the grating is oriented correctly and the light and dark bars are positioned over the ON and OFF subregions, respectively (DeAngelis et al., 1993; Wielaard et al., 2001). In contrast, the position of the stimulus does not dictate the response of a complex cell, although they are still sensitive to the orientation of a stimulus.

There are fewer orientation selective cells in mouse V1 compared to cats and primates, and cells that are selective have broader tuning curves (Mangini & Pearlman, 1980; Livingstone, 1998; Niell & Stryker, 2008). It has been shown in mouse V1 that roughly 40% of neurons are orientation selective (Dräger, 1975b; Mangini and Pearlman, 1980; Niell and Stryker, 2008; Gao et al., 2010), with some neurons showing no preference at all. In primates, it is estimated that about 90% of neurons have a preference for orientation (Hubel and Wiesel, 1959, 1974; Schiller et al., 1976).

1.4.2 Spatial and Temporal Frequency

In vision research, the primary stimulus used has been the sine wave grating because its luminance shift over both space and time can be easily described using a sinusoidal function (Enroth-Cugell and Robson, 1984). For these gratings, the spatial frequency (SF) is the number of cycles in one degree of visual angle at the eye, and it is measured in cycles per degree (cpd). The temporal frequency (TF) describes how many cycles are completed per unit of time, and is measured in cycles per second or Hertz (Hz). Tuning functions for SF and TF have been described in both macaque and mouse V1

neurons (De Valois et al., 1982; Foster et al., 1985; Hawken et al., 1996; Niell and Stryker, 2008; Gao et al., 2010).

In the macaque, behaviourally measured visual acuity for features viewed with the fovea has a threshold of ~38cpd (Merigan and Katz, 1990), and electrophysiological studies have shown that the preferred SFs and TFs of V1 neurons range from 1.9-3 cpd and 7.8-8Hz, respectively (Foster et al., 1985; Bair and Movshon, 2004). Comparatively, mice have far worse visual acuity with a psychophysical threshold of ~0.5cpd (Prusky et al., 2000). However, even though their acuity is low, mouse V1 neurons have robust SF and TF tuning (Niell and Stryker, 2008; Gao et al., 2010; Andermann et al., 2011; Marshel et al., 2011). Niell and Stryker (2008) reported that mouse V1 cells prefer SFs ranging from 0.02-0.08 cpd, with a median preferred SF of 0.036 cpd. Gao et al. (2010) report similar results, with neurons preferring SFs from 0.02-0.09 cpd, with the median preferred being 0.03 cpd. Marshel et al. (2010) utilized two-photon *in vivo* calcium imaging to look at the tuning properties in anesthetized mice and reported a mean preferred SF of 0.045 cpd in V1 cells.

In mouse V1, Gao et al. (2010) determined that the median preferred TFs were within the range of 1.2-1.9Hz, which agrees with the value reported by Niell and Stryker (2008) of 1.68Hz. Marshel et al. (2010) reported a value of 0.69Hz in mouse V1 neurons, but the difference may be because they used calcium imaging whereas Neill and Stryker (2008) and Gao et al. (2010) used single-unit electrophysiology.

1.5 OBJECTIVE OF THE CURRENT EXPERIMENTS

Visual adaptation is of interest to the scientific community for two reasons (for review, see Kohn 2007). The first is because it is a form of short-term plasticity. The visual system is an ideal sensory system to utilize adaptation research as it can be quickly induced, and takes little time for reversal (i.e. control and experimental trials can be run quickly). Although all forms of plasticity employ different mechanisms, there are overlapping research goals between fields such as determining benefits of plasticity, linking neuronal plasticity to perceptual experiences, and determining if there is a uniform circuit organization that is present in different sensory modalities. The second reason is because the effects of adaptation effect sensory perception in real time, and therefore must be a necessary part of sensory processing.

Visual adaptation in mice is a new field of research. The studies performed thus far on contrast adaptation (e.g. Stroud et al., 2012; LeDue et al., 2013) have provided promising evidence that this phenomenon manifests similarly in mouse V1 as in cats and primate. The two projects within this thesis examine two different types of visual adaptation, namely orientation adaptation and contrast adaptation. The results from both studies suggest that there are similarities in visual neural circuitry between mice and more traditional models of vision as we observed similar changes in neuronal tuning curves in mouse V1 as has been previously reported in cats and primates.

1.5.1 Experiment 1: Adaptation to Stimulus Orientation in the Mouse Primary Visual Cortex

The first project examines adaptation to stimulus orientation in mouse V1. Orientation adaptation was of interest for two reasons: 1) it has yet to be thoroughly

quantified and described in the mouse visual system, and 2) we were curious as to how it would manifest in mice as they lack pinwheel organization in V1, and have fewer orientation selective neurons. To accomplish this, mouse V1 neurons were adapted to an oriented sine wave grating and changes in peak location, bandwidth and amplitude were quantified from the resulting tuning curves.

1.5.2 Experiment 2: Contrast Adaptation in Mouse V1 Depends on Spatial Frequency but Not On Spike Rate

The second project is a continuation of work we previously published on mouse contrast adaptation (LeDue et al., 2013) which demonstrated that contrast adaptation in mouse V1 is specific in the spatiotemporal domain. It was shown that the magnitude of adaptation was significantly affected by the SF and TF of the adapting stimulus. We reported that when a neuron was adapted and tested with identical stimuli the magnitude of adaptation was greater than when the adapting stimulus did not match the test grating. However, the overall spike rate was not controlled for in this study, and as such it could be argued that the reason we observed differing amounts of adaptation was not due to altering SFs or TFs of adapting stimuli, but was rather the result of differences in elicited spike between the adapting and testing stimuli. Therefore, the second project in this thesis corrects this issue as we choose two SFs that elicited similar spike rates. Due to the more careful selection of SFs, any differences observed in the contrast response functions after adaptation can more confidently be attributed to the differences in SF.

CHAPTER 2: ORIENTATION PLASTICITY IN MOUSE V1

2.1 Introduction

Vision has a memory. Many studies of sensory adaptation and/or aftereffects suggest that the visual system possesses a number of mechanisms to calibrate itself based on what has been viewed in the recent past (for reviews see Carandini, 2000; Kohn, 2007). Adaptation to the orientation of an edge or texture is especially interesting because unlike brightness, color, or contrast, this process is thought to emphasize V1 and extrastriate areas since antecedent stages of analysis show little selectivity for orientation (but see Smith et al., 1990; Xu et al., 2002; Kuhlmann and Vidyasagar, 2011). In the tilt-aftereffect and similar visual illusions, prolonged viewing of an adaptor grating causes the orientation of the subsequently presented test grating to appear shifted away from (or 'repelled' by) the adaptor's orientation (Gibson and Radner, 1937; Levinson and Sekuler, 1976; Patterson and Becker, 1996; Schrater and Simoncelli, 1998; Clifford, 2002). A potential neural correlate for these perceptual effects has been described in cat and macaque, where adaptation within the classical receptive field of V1 neurons produces repulsive shifts in the orientation tuning curves of these cells (Dragoi et al., 2000, 2001; Wissig and Kohn 2012; Patterson et al., 2013). Recent electrophysiological studies in cats and macaques have made progress in establishing how several aspects of the stimulus protocol can affect the nature of orientation adaptation (including: duration of adaptation, the adapting angle, and stimulus size), but there are many remaining details to be revealed about the neural mechanisms underlying this form of short-term plasticity

A version of this manuscript has been submitted to The Journal of Neurophysiology:
King JL, Crowder NA, Adaptation to Stimulus Orientation in the Mouse Primary Visual Cortex, manuscript #JN-00819-2014 (Oct 2014).

(Dragoi et al. 2000; Ghisovan et al., 2009; Wissig and Kohn, 2012; Patterson et al., 2013).

Several powerful genetic tools most readily applied in transgenic mice could potentially provide insight into the neural circuitry and plasticity underlying adaptation, so the aim of the present study was to establish a baseline description of orientation adaptation in this species. Despite mice having spatial acuity up to two orders of magnitude lower than classical animal models of vision (Wong and Brown, 2006), their V1 neurons share many features with those of more visual species including: tuning for spatial and temporal frequencies; presence of simple and complex cells; binocular disparity selectivity; and most relevant for the current work, selectivity for orientation and direction (Niell and Stryker, 2008; Gao et al., 2010; Van den Bergh et al., 2010; Scholl et al., 2013). Studying orientation adaptation in mice is also interesting from a comparative perspective because there appears to be at least three differences in the way orientation information is dealt with in mouse V1 compared to classical models. First, there is a larger proportion of neurons that are not selective for orientation in mouse V1 (Niell and Stryker, 2008; Gao et al., 2010; Stroud et al., 2012). Second, there is evidence that orientation selectivity emerges prior to V1 in the mouse, and the sharpening of orientation tuning as signals pass between the dorsal lateral geniculate nucleus (dLGN) to V1 is not as dramatic as in cats and primates (Scholl et al., 2013, but see Lien and Scanziani, 2013). Finally, whereas cats and primates have columns of orientation selective V1 neurons organized into iso-orientation domains that converge in pinwheel centers, mice lack this organization (Ohki et al., 2005).

To determine whether stimulus history can change the orientation tuning of mouse V1 neurons, we used single unit recording and adaptation paradigms that were comparable with previous studies in cat and monkey (Wissig and Kohn, 2012; Patterson et al., 2013). We found that most orientation selective units in our sample showed repulsive shifts in their tuning curves following adaptation, and comparisons to other species will be considered. We also found that adaptation caused attenuated responses across all orientations in both orientation selective cells and those not tuned for orientation, an effect which appears to be unique to mice.

2.2 **Materials and Methods**

2.2.1 *Animals*

Experiments were performed on male C57BL/6J mice between 2 and 7 months of age and weighing between 22 and 33g. All experimental procedures were performed in accordance with the guidelines of the Canadian Council on Animal Care and were approved by the Dalhousie University Committee on Laboratory Animals.

2.2.2 *Preparation*

Animals were pre-medicated with an injection of chlorprothexine (5mg/kg I.P.; Sigma Aldrich), then placed in a custom face-mask and anesthetized with isoflurane in oxygen for the remainder of the experiment (2.5% isoflurane during induction, 1.5% during surgery, and 0.5% during recording; Pharmaceutical Partners of Canada). Additional doses of chlorprothexine were given every four hours. Once anesthetized, mice were maintained at a body temperature of 37.5^{o}C with a heating pad, and their

corneas were protected by frequent application of optically neutral silicone oil (30,000 cSt, Sigma Aldrich).

In preparation for electrophysiological recordings, the scalp was removed and a head post was secured using dental epoxy. A small craniotomy (~1mm^2) was then made 0.8mm anterior and 2.3mm lateral from lambda (Paxinos and Franklin, 2001). A well made from petroleum jelly surrounded the craniotomy, and was filled with saline to prevent dehydration of the cortex. Extracellular recordings were made with glass micropipettes containing 2M NaCl, with a tip diameter of 2-5µm. Signals from individual units were isolated, amplified, filtered, and acquired with a CED 1401 interface and Spike2 software (Cambridge Electronic Designs, Cambridge, UK) sampled at 40kHz. Online responses were generated in Spike2 from triggered transistor-transistor logic (TTL) pulses from a window discriminator (Cornerstone by Dagan), but spike sorting and all further analyses were performed offline (see LeDue et al., 2013 for details).

2.2.3 *Visual Stimuli*

Once a visually responsive neuron was isolated, the receptive field (RF) was mapped by hand using an ophthalmoscope. Quantitative stimuli, which were programmed in MATLAB (Math Works, Natick, MA) using the Psychophysics Toolbox extension (Brainard, 1997; Pelli, 1997), were presented on a calibrated CRT monitor (LG Flatron 915FT Plus 19 inch display, 100 Hz refresh, 1024 x 768 pixels, mean luminance = 30cd/m^2) at a viewing distance of 25-30cm. Each unit's preferred orientation, RF size, SF, and TF were analysed online to ensure robust responses during the orientation adaptation protocol. All stimuli were presented for 8-12 repetitions. Orientation tuning was tested with square-wave gratings (SF = 0.03 cycles per degree (cpd); TF = 2 Hz)

moving back-and-forth along 8 orientation axes. Preferred size was tested with both sine-wave gratings in different sized circular apertures, and a full field grating with a circular aperture of grey at its center. These two stimuli not only allowed the size tuning of the neuron to be tested, they also facilitated centering of the monitor over each neuron's receptive field. The size of the circular aperture used for all subsequent stimuli was usually chosen as either the diameter where the size tuning function began to asymptote in neurons lacking surround suppression, or the peak of the size tuning function for neurons that showed surround suppression. Tuning for spatio-temporal frequency was measured with sine wave gratings drifting in the preferred direction presented at 36 different combinations of SF (0.01, 0.02, 0.04, 0.08, 0.16, 0.32 cpd) and TF (0.25, 0.50, 1, 2, 4, 8Hz), and the start phase of each repetition was staggered to ensure responses could be measured in phase-sensitive neurons even at low TFs (see LeDue et al. 2012, 2013).

Orientation Adaptation

For the orientation adaptation protocol, orientation tuning was measured with 11 test angles spanning 180^{o} centered on the unit's preferred direction as determined from the online analysis. Each test grating was shown for 2s. On adaptation trials this test grating was preceded by a 2s adaptor grating, whereas on non-adaptation trials this test grating was preceded only by a grey of mean luminance. Adapted and non-adaptation trials were randomized, and a grey of mean luminance was shown for the 6s interstimulus interval between trials. We used the unit's preferred SF and TF if sine wave gratings were used in the adaptation protocol or an SF of 0.03cpd and TF of 2Hz if square wave gratings were used.

2.2.4 *Data Analysis*

The least squares method was used to fit each orientation tuning curve to a von Mises function, which is a circular Gaussian often used in modeling orientation tuning (e.g. Swindale, 1998):

$$r_p(\theta) = m + ae^{b(\cos(\theta-\theta pref)-1)} \quad (1)$$

where the response (r_p) at a given angle (θ) is the determined by the bandwidth (b) and preferred orientation (θ_{pref}), amplitude (a) and baseline response rate (m). The goodness of fits were calculated with R^2. Each unit's selectivity for stimulus orientation was also quantified using a discrimination index (D.I.), which accounts for both depth of tuning and the variability of responses (DeAngelis & Uka, 2003):

$$\text{D.I.} = \frac{\text{Resp}_{\text{Max}} - \text{Resp}_{\text{Min}}}{\text{Resp}_{\text{Max}} - \text{Resp}_{\text{Min}} + 2\sqrt{\text{SSE}(N-M)}} \quad (2)$$

Resp_{Max} and Resp_{Min} are the maximum and minimum responses of the neuron in spikes per second, SSE is the sum of square error, N is the total number of stimuli presented, and M is the number of different stimuli. In order for a unit to be classified as orientation selective, both adapted and nonadapted curves had to have D.I. $\geq$ 0.425 (an arbitrary cutoff that usually corresponded to approximately 2:1 modulation), and von Mises fits with $R^2 \geq 0.5$. Neurons that did not reach criterion to be classified as orientation selective were also fitted to a straight line, and an F-test was used to compare von Mises and linear fits:

$$F = \frac{(SS_l - SS_v) / (df_l - df_v)}{(SS_v)/(df_v)} \quad (3)$$

SS_v and SS_l are the residual sum of squares for the von Mises fit and linear fits,

respectively. The degrees of freedom for the von Mises (df_v) and linear fits (df_l) were calculated as the number of data points minus number of parameters being estimated. A p-value was then calculated to determine whether the von Mises curve fit the data significantly better than a straight line.

The final analysis quantified how many phase sensitive neurons were in our sample using the F_1/F_0 ratio. The F_1/F_0 ratio is determined by dividing the first Fourier coefficient of the response (F_1) by the mean time-averaged response (F_0). This F_1/F_0 ratio has been used in classical animal models of vision to categorize orientation tuned V1 neurons as simple (>1) or complex types (<1; Skottun et al. 1991). Here we use the nomenclature of phase-sensitive ($F_1/F_0 > 1$) and phase-invariant ($F_1/F_0 < 1$) because not all of the units in our sample were orientation selective.

For statistical comparisons we performed Wilcoxon sign rank tests for repeated measures, and rank sum tests for comparisons groups. We applied Bonferroni corrections to account for multiple comparisons.

2.3 **Results**

Orientation adaptation was tested in 106 units, of which 42 exceeded the threshold to be classified as orientation tuned, whereas 56 did not. We also observed a sample of 8 cells that fit the criteria to be classified as tuned before adaptation, but after adaptation the peaks of their tuning curves disappeared. This loss of peak cannot be attributed to losing isolation of the unit because non-adaptation and adaption trials were randomized. Our sample contained 22 phase-sensitive and 84 phase-invariant units, but

the effects of orientation adaptation were similar between these two groups, so they were pooled for subsequent analysis.

2.3.1 *Orientation Tuned Neurons*

Peak Shift

The most frequently reported effect of orientation adaptation on orientation selective neurons in previous literature using cats or monkeys is a shift in the preferred orientation of the adapted tuning curve. Here we defined the peak shift as the difference between the adapted and non-adapted θ_{pref} parameters extracted from the Gaussian fits. Peak shifts were classified as repulsive when the adapted peak shifted away from the adapt angle (n=23), and attractive when the adapted peak shifted towards the adapt angle (n=13). Some neurons in our sample also showed virtually no peak shift after adaptation (<1°, n=6). Figure 1A shows data for a cell that demonstrated a repulsive shift after adaptation, and figure 1B shows data for a cell that had an attractive shift. In our tuned sample the peaks of only 3 neurons shifted more than 20° from the adapt angle, with the remaining 38 shifting ≤15°.

When selecting the angle of each adaptor from the online tuning curve, we attempted to pick an orientation that was on the flank of the tuning curve midway between the peak and where the curve returned to baseline. We were able to flank-adapt 28 units, but 14 other units had an adaptor angle beyond the strongly sloped section of the tuning curve, which we will refer to as undergoing end-of-flank adaptation following Kohn and Movshon (2004). The distinction between flank and end-of-flank adaptation is important because it has been previously shown in primates that flank adaptation causes

mainly repulsion whereas the effects of end-of-flank adaptation are more variable (Wissig and Kohn, 2012; Patterson et al., 2013). For our sample of flank adapted neurons, 7 cells had an attractive shift, 16 were repulsive, and 5 did not shift. For the end-of-flank adapted neurons, 6 had an attractive shift after adaptation and 8 showed repulsive shifts. Figure 1C shows a histogram of the population data, with flank adapted neurons and end-of-flank adapted neurons in black and grey bars, respectively. Mean peak shifts for flank adapted (-5°) and end-of-flank adapted (+2.1°) are indicated on figure 1C as black and grey diamonds, respectively. Flank adaptation produced significant repulsion ($p = 0.02$), but end-of-flank adaptation did not cause repulsion or attraction consistently ($p = 0.76$).

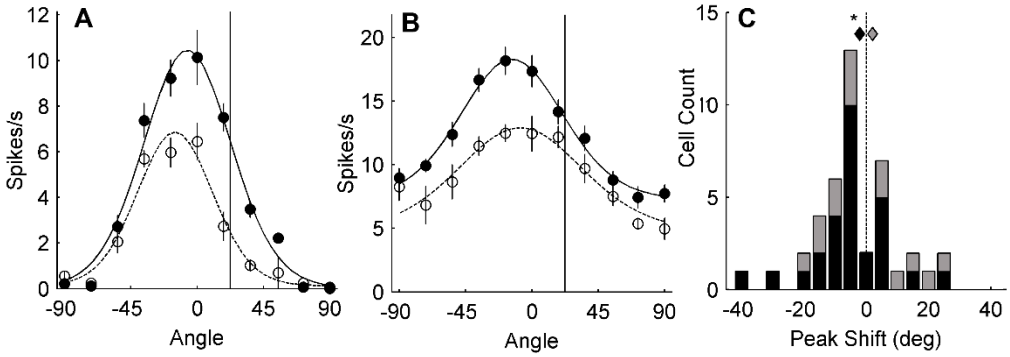

Figure 1: Peak shift in orientation selective neurons. *A-B:* tuning curves from two example neurons showing repulsive (*A*) and attractive (*B*) shifts. On the abscissa are the test grating angles, with 0° being the neuron's preferred orientation, and on the ordinate is the neuron's response in spikes/second. The solid tuning curve with filled-in circles is the cell's response before adaptation, and the dashed tuning curve with empty circles is the cell's response after adaptation to the angle indicated by the vertical line. Error bars are SEM. *C*: A histogram showing the peak shifts of all tuned neurons in our sample, with negative values indicating repulsive shifts and positive values indicating attractive shifts. Flank adapted neurons and end-of-flank neurons are black and grey bars, respectively. Mean peak shifts are shown by the diamonds in corresponding colours.

Amplitude

It is apparent from the cells in figure 1A,B and 2A that tuning curves are shifted to lower firing rates following adaptation. Nonadapted baseline and peak firing rates from von Mises functions were compared to their corresponding adapted values to measure the change in neurons' responsivity following adaptation. The vast majority of our sample had a lower spike rate after adaptation, regardless of whether they were flank or end-of-flank adapted. The histograms in figures 2B and C show the percent change in peak and baseline firing, respectively, with negative numbers indicating a reduction in spike rate. Flank adapted and end-of-flank adapted neurons are shown as black bars and grey bars, respectively. There was a significant decrease in spike rate for both the peak ($p<0.0001$) and baseline spike rates ($p<0.0001$) in both groups of neurons. The scatterplot in figure 2D compares the change in baseline spike rate with the change in peak spike rate, with black and grey data points indicating flank and end-of-flank adapted neurons, respectively. These two measures were moderately correlated ($r = 0.65$), but the majority of the data points were below the line of equality, indicating that adaptation caused a larger decrease in firing at the peak of the tuning curves, and this difference was significant ($p=0.001$). Past studies of orientation adaptation have not commonly reported changes in tuning curve amplitude, but the few studies that have quantified this effect reported little change following flank adaptation or facilitation following end-of-flank adaptation (Dragoi et al., 2000, 2001; Wissig & Kohn, 2012; Patterson et al., 2013).

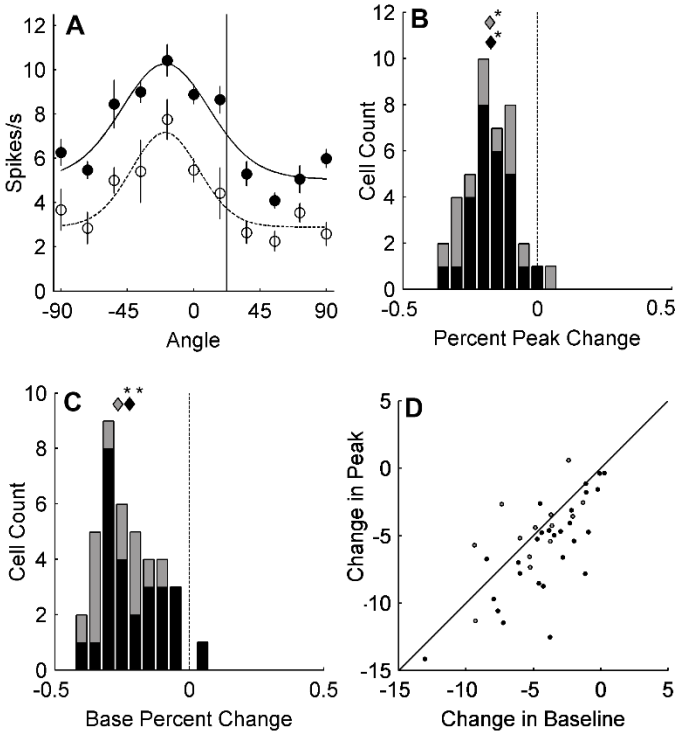

Figure 2: Amplitude changes in orientation selective neurons. *A*: An example of a tuned neuron showing a decrease in response to all test angles after adaptation. The format is identical to that in figure 1. *B*-*C*: Histograms showing the percent change in the maximum (*B*) and minimum (*C*) response after adaptation in all tuned cells. Negative values indicate decreases in response and positive values increases in response. The colour format is identical to that in figure 1, with diamonds showing the mean decrease. *D*: A scatterplot comparing the change in baseline spiking to the change in peak spiking, with black and grey dots indicating flank and end-of-flank adapted neurons, respectively.

Bandwidth

Bandwidth of the orientation tuning curve was defined as the full width of the curve at half the elevation above baseline. The example cell in figure 3A shows a flank adapted neuron whose tuning curve narrowed after adaptation. The mean bandwidth in our sample was 66.2° before adaptation and 63.2° after adaptation. The histogram in figure 3B shows bandwidth change, with flank adapted and end-of-flank adapted neurons

in black and grey, respectively. In our sample, 22 tuning curves narrowed (16 flank and 6 end-of-flank), 18 widened (10 flank and 8 end-of-flank), and 1 flank adapted neuron had no change in bandwidth (<1°). Mean bandwidth changes for flank (-8.54°) and end-of-flank (+2.42°) adapted are shown as black and grey diamonds, respectively. However, bandwidth changes were not consistent enough to produce a statistically significant effect at the population level (p=0.08 for flank adapted neurons, p=0.9 for end-of-flank adapted cells).

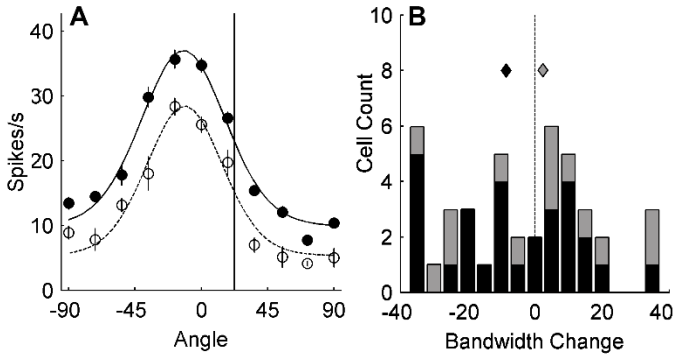

Figure 3: Bandwidth changes in orientation selective neurons. *A*: An example of a tuned neuron whose tuning curve narrowed after adaptation. Format is the same as in figure 1. *B*: A histogram showing the changes in bandwidth after adaptation for all cells in our tuned sample. Negative and positive numbers indicate narrowing and widening, respectively. Colour scheme is identical to figure 1, with diamonds indicating the mean changes.

2.3.2 *Neurons not tuned for orientation*

The remaining 56 cells in our sample were not strongly selective for orientation, and therefore classified as non-oriented. Only 2 neurons in this sample (4%) had non-adapted and adapted curves that were fit significantly better to a von Mises function

compared to a straight line, therefore analyses were performed using values obtained from the line-of-best-fit. Studies on orientation adaptation in cat and monkey have not included much data on non-oriented neurons, but these cells are much more prevalent in mouse V1 (Niell and Stryker, 2008; Gao et al. 2010; Stroud et al. 2012), so we used adaptation as a way to investigate why these cells lack orientation selectivity. We had two models as to how orientation adaptation might affect non-oriented neurons. In the first model, non-oriented neurons pool inputs from multiple tuned neurons, so adaptation at a single orientation would be expected to decrease the drive only from afferents responsive to the adaptor, thereby producing a dip in the neuron's adapted tuning curve at the adapt angle (Figure 4A). A recent study in macaque V1 did indeed show this selective decrease in firing at the adaptor angle, but it was accompanied by facilitation at other test angles (Wissig and Kohn 2012). In the second model, non-oriented V1 cells do not receive orientation selective inputs (either from the dLGN or cortex), so adaptation at any angle produces a generalized decrease in firing to any adaptor angle (Figure 4B). Our untuned sample supports this second model. Figure 4C shows an example of an untuned neuron, and the overall decrease in its response is quite obvious. A dip at the adaptor angle following adaptation would have been well fit by a von Mises with negative amplitude, but this was never observed. Figure 4D shows a histogram of the percent change of the minimum response from the linear fits. Black bars indicate cells that were untuned both before and after adaptation, and grey bars indicate cells which lost tuning after adaptation. The decrease in minimum firing after adaptation was significant for both untuned neurons and units that lost tuning, and the mean decrements are shown as black and grey diamonds, respectively ($p<0.00001$ for both groups).

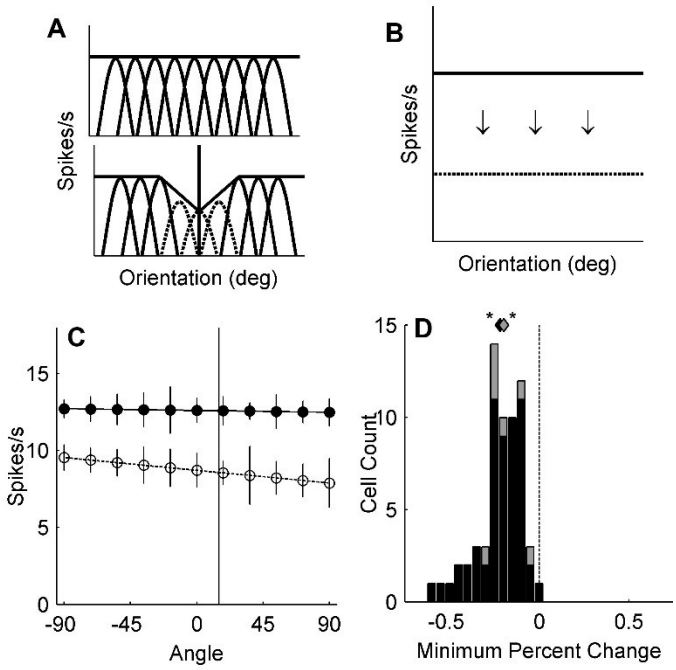

Figure 4: Untuned neurons. *A*: The first model we hypothesized how orientation adaptation might manifest in neurons not selective for orientation. If untuned neurons receive inputs from multiple tuned cells (top panel) than we would expect adaptation to cause a selective dip at the adapt angle (bottom panel). *B*: The second model, if non-oriented cells only receive non-oriented inputs, then adaptation would cause a general decrease in response to all test angles. *C*: An example of an untuned neuron. Format is the same as in figure 1. *D*: A histogram showing the percent change in the minimum response of our untuned sample, with negative values indicating a decrease in response. Black and grey bars are untuned cells and the 8 cells that lost tuning after adaptation, respectively. The corresponding coloured diamonds indicate the mean decrease in minimum spiking.

2.4 **Discussion**

The change in orientation tuning of V1 neurons following prolonged exposure to a single orientation is a well-known example of adaptation that has been studied in classical animal models of vision (cats: Priebe et al. 2010; Bachatene et al. 2012; Cattan et al. 2014; monkeys: Wissig and Kohn, 2012; Patterson et al. 2013), and here we sought to determine whether orientation adaptation is also apparent in mouse V1. Every neuron

in our sample showed some evidence of adaptation: flank adaptation caused mostly repulsive shifts in orientation selective V1 neurons, whereas the effects of end-of-flank adaptation were more varied. Furthermore, nearly every cell showed an attenuation of firing rates across all orientations following adaptation.

2.4.1 *Comparisons with Previous Studies*

We are confident that our results are representative of adaptation in mouse V1 because the nonadapted orientation tuning curves in our population were comparable to previous studies of this brain area. We found that 42% of neurons were reliably modulated by orientation, which is close to the estimate of 48.5% given by Gao et al. (2010) using similar methods. The median bandwidth of orientation tuned cells in our sample was 69.75°, which falls within range of median bandwidths reported by previous studies (58° from Niell and Stryker 2008; 86° from Gao et al. 2010). Approximately 21% of the units in our sample were phase-sensitive, which is higher than the 6% reported by Gao et al. (2010), but lower than the ~35-50% reported in other studies (Niell and Stryker 2008; Van den Bergh et al. 2010). This variability likely reflects a sampling bias (especially considering the multi-site silicone probe and stimulus protocol used by Niell and Stryker (2008) allowed the sampling of very sparsely responding units), but is unlikely to be problematic for the interpretation of our results because both phase-sensitive and phase-invariant units showed adaptation.

All previous studies of orientation adaptation in cats and monkeys have measured how the peak of the tuning curve shifts following adaptation. For flank adaptation that predominantly targets the classical receptive field, a repulsion away from the adapting orientation is the most common effect, and the mean magnitude of this peak shift ranges

from 2 – 9^{o} (Dragoi et al., 2001; Wissig and Kohn, 2012; Patterson et al. 2013; Ghisovan et al. 2009). Therefore, the average repulsion of 5^{o} we observed under similar stimulus conditions in mice is quite comparable. In macaques, the magnitude of the peak shift was only weakly affected by prolonging the adaptation time from 0.4s to 40s (Patterson et al. 2013), so we are confident that our adaptor duration of 2s was sufficient to capture the main effects of adaptation. Several studies in opioid-anesthetized macaques have found that repulsive shifts are supplanted by attraction when the stimulus is large enough to extend into the extraclassical receptive field of most V1 neurons, and this effect has been modeled as an orientation tuned input divisively suppressed by a similarly tuned surround in an orientation-specific manner (Kohn and Movshon, 2004; Wissig and Kohn, 2012; Patterson et al. 2013). We observed some attractive shifts in our population, but we doubt that they are related to the aforementioned extraclassical mechanism for two reasons. First, we attempted to limit stimuli to the classical receptive field. Second, it has been reported that isoflurane-urethane anesthesia decreases surround suppression in mice (Adesnik et al. 2012; Vaiceliunaite et al. 2013), so extending our stimuli into the extraclassical receptive field probably would only provide weak drive to this surround mechanism.

One of the largest differences in V1 organization between rodents and other animal models is the columnar organization of orientation selectivity (Van Hooser et al. 2005). In carnivores and primates, orientation selective neurons whose retinotopic receptive fields cover a particular region of space are clustered into iso-orientation domains, which converge at pinwheel centers (Bonhoeffer and Grinvald, 1991; Maldonado, 1997; Dragoi et al. 2001; Nauhaus et al. 2008). Although adjacent neurons in

pinwheel maps can have vastly different orientation preferences, anatomical studies show that the local dendritic arbours of these V1 neurons have a circularly symmetrical geometry and extend approximately 500-800μm into surrounding cortex independent of the somatic position on the orientation map (Malach et al. 1993; Das and Gilbert, 1999; Levy et al. 2014). Therefore the local network inputs to an individual V1 neuron will depend on its location within this map. Orientation tuning has been shown to be more broad at pinwheel centers (Nauhaus et al. 2008), and an adaptation study in cats found that neurons located at pinwheel centers shifted their orientation preference by an average of 12° following adaptation whereas the mean shift for cells in iso-orientation domains was 3° (Dragoi et al. 2001). Both of these findings are hypothesized to reflect the inhomogeneous local network signal across the orientation map. The salt-and-pepper organization of mouse V1 might create a local network where each cell receives inputs from neighbors of many orientation preferences, akin to the neurons in pinwheel centers of cats or primates, and therefore orientation adaptation should be homogeneously robust in mouse. Consistent with this line of reasoning, mouse V1 neurons are also broadly tuned compared to their counterparts in cats and primates (Niell and Stryker 2008; Gao et al. 2010). We were therefore surprised to find more modest average peak shift for the population as well as significant variability in shift amplitudes.

We were also surprised by the consistency and magnitude of the broadly tuned response attenuation following adaptation. For orientation tuned cells, the firing rates decreased more at the peak of the tuning curve than at orthogonal orientations, which suggests divisive rather than subtractive gain control (Nowak and Barone, 2009; Schwartz et al. 2009). Divisive gain control is when the amplitude of a curve is divided

by a constant value, which will lead to larger changes at the peak of the curve and smaller changes on the flanks. Subtractive gain control is when curve is decreased by a set amount throughout its entirety, which causes a downward shift without altering the shape of the curve. Many neurons in mouse V1 have a so-called "untuned baseline response" above the spontaneous rate even to stimuli orthogonal to the preferred orientation (Niell and Stryker, 2008), which may have made the breadth of the adaptation induced attenuation especially conspicuous. Such overall response attenuation has not been reported in cats or primates, and in fact end-of-flank adaptation has actually been shown to cause facilitation (Dragoi et al. 2000, 2001; Wissig and Kohn, 2012; Patterson et al. 2013). Adaptation in non-oriented cells also appears to follow different patterns in mice and primates. We found evidence that adaptation of non-oriented neurons in mice is at least partially derived from adaptation of untuned afferents (figure 4B-D), whereas the orientation specific attenuation observed in macaques indicates non-oriented cells in this species are probably pooling multiple oriented inputs (Wissig and Kohn, 2012).

2.4.2 *Implications for future work*

One of the goals of visual neuroscience is ultimately to link perception to underlying neural activity, and it seems obvious that this endeavor should require multiple levels of analysis. For orientation adaptation in particular, single unit electrophysiology studies in awake behaving primates probably offer the best chance for linking psychophysical phenomena like the tilt illusion or the tilt after-effect with altered orientation tuning curves in various visual areas (Patterson et al., 2014). However, attempts to identify relevant neural circuits or the role of particular cell types in adaptation may benefit from using genetic tools that are most easily applied in mice.

Transgenic mouse lines expressing Cre or similar tools (Runyan et al. 2010; Cai et al. 2013) have facilitated the labelling, targeted recording, and optogenetic control of specific cell types. For example, both parvalbumin- and somatostatin-expressing GABAergic interneurons have been proposed to play a role in V1 surround suppression (Adesnik et al. 2012; Vaiceliunaite et al. 2013), which has been hypothesized to influence orientation adaptation in several ways in primates (Wissig and Kohn, 2012; Patterson et al. 2013). Although some species differences are likely inevitable, an advanced understanding of the circuits underlying adaptation in mice will undoubtedly allow for more targeted questions in models of vision more similar to humans.

CHAPTER 3: CONTRAST ADAPTATION IN MOUSE V1 IS DEPENDENT ON SPATIAL FREQUENCY IN ADDITION TO SPIKE RATE

3.1 Introduction

Visual adaptation plays a large role in how we perceive our environment. Many aspects of a stimulus are subject to adaptation, such as contrast, orientation, and spatial and temporal frequency (Movshon et al., 1978; Duong and Freeman, 2007). Spatial contrast is the difference in luminance between parts of an object or scene and is thought to be an important stimulus parameter for the visual system as early as center-surround antagonism in the retina (Carandini et al., 2005). Perceptually, contrast adaptation causes a perceived fading of the adapting stimulus and a reduced sensitivity to low contrasts, but it can also cause an increase in sensitivity around the adapting contrast (Blakemore and Campbell, 1969; Greenlee and Heitger, 1988; Foley and Chen, 1997; Abbonizio et al., 2002). V1 neurons have a sigmoidal contrast response function when spike rate is plotted as a function of stimulus contrast, and contrast adaptation causes this curve to shift downwards and towards the adapting contrast (Movshon and Lennie, 1979; Ohzawa et al., 1982, 1985; Sclar et al., 1989; Bonds, 1991; Ibbotson, 2005).

Perceptual studies have shown that contrast adaptation is pattern-specific, such that the magnitude of contrast adaptation is dependent on the similarity of the SF, TF and orientation of the adapting and test stimuli (Carandini et al., 1998; Carandini, 2000). The mechanisms behind this pattern specificity are only beginning to be uncovered. For example, the magnitude of contrast adaptation measured in cat LGN neurons does not depend on the SF of the stimulus, but in V1 adaptation is strongest when the SF of the adapting and test gratings match. (Movshon and Lennie 1979; Duong and Freeman, 2007).

Over the past decade the mouse has become an increasingly popular visual model due to the genetic tools available. Although mice have an order of magnitude lower acuity than more traditional animal models, it has been demonstrated that mice V1 neurons also have sigmoid contrast response functions and that contrast adaptation in mouse V1 causes these functions to shift downwards and towards the adapting contrast (Stroud et al., 2012). As such, mice provide a unique opportunity to study the mechanisms behind contrast adaptation as their neural networks can be accurately perturbed in a manner not attainable pharmacologically. But first, expansion on more baseline studies and comparisons to previous work in cat and primates are required.

A recent study performed by LeDue et al. (2013) altered either the SF or TF of the adapting stimulus, and demonstrated that the magnitude of adaptation was significantly less when the adapting grating did not match the test grating. These findings provide evidence that contrast adaptation in mouse V1, like in cat and primate V1, is specific in the spatiotemporal domain. However, LeDue et al. (2013) did not control for spike rate. When neurons were adapted and tested with identical gratings they chose preferred stimuli parameters, thereby causing the neuron to spike maximally. In the conditions when they altered the SF or TF of the adapting grating they chose non-preferred parameters, therefore the neuron responded less. Because the neuron elicited fewer spikes during adaptation when they altered the SF or TF, the decreased magnitude of adaptation could have been the result of neural fatigue, not the difference in stimuli.

To disambiguate fatigue-like effects from pattern specificity we controlled for spike rate by choosing SFs for adapting and test gratings that evoked similar spike rates in a particular neuron. We found that the magnitude of adaptation was greatest when the

SF of the test matched the adapting grating, even though both adapting gratings elicited similar spike rates. These findings, taken together with the work of LeDue et al. (2013), suggest that contrast adaptation in mouse V1 is pattern selective.

3.2 Methods

3.2.1 *Animals*

Experiments were performed on male C57BL/6J mice, aged 2-7 months, weighing between 22 and 33g (n = 14). All experimental procedures were performed in accordance with the guidelines of the Canadian Council on Animal Care and were approved by the Dalhousie University Committee on Laboratory Animals.

3.2.2 *Preparation*

Animals were pre-medicated with an injection of chloprothexine (Sigma Aldrich, 5mg/kg, i.p.), then placed in a custom face-mask and anesthetized with isoflurane in oxygen for the remainder of the experiment (2.5% isoflurane during induction, 1.5% during surgery and 0.5% during recording, Pharmaceutical Partners of Canada). Additional doses of chlorprothexine were given every four hours. Once anesthetized, mice were maintained at a body temperature of 37.5^{o}C using a heating pad, and their corneas were protected by hourly application of optically neutral silicone oil (30,000 cSt, Sigma Aldrich).

To expose V1, the scalp was first removed and then a head post was secured using dental epoxy. A craniotomy (~1mm^2) was then made 0.8mm anterior and 2.3mm lateral from lambda (Paxinos and Franklin, 2001), and a small well composed of petroleum jelly was filled with saline to prevent the dehydration of the surface of the V1. Extracellular

recordings were made with glass micropipettes that were filled with 2M NaCl and had a tip diameter of 2-5µm. Signals from individual cells were isolated, amplified, filtered and acquired with a CED 1401 interface and Spike2 software (Cambridge Electronic Designs, Cambridge, UK) sampled at 40kHz. Online responses were generated from TTL pulse in Spike2 from a window discriminator (Cornerstone by Dagan), but spike sorting and all subsequent analyses were performed offline.

3.2.3 *Visual Stimuli*

Once a visually responsive neuron was isolated, the RF was mapped manually using an ophthalmoscope. Stimuli, programmed in MATLAB (Math Works, Natick, MA) using the Psychophysics Toolbox extension (Brainard, 1997; Pelli, 1997), were presented on a calibrated CRT monitor (LG Flatron 915FT Plus 19 inch display, 100 Hz refresh, 1024 x 768 pixels, mean luminance = 30cd/m^2) at a viewing distance of 25-30cm. All stimuli except for one were presented in a circular aperture surrounded by a grey field of mean luminance. The first four stimuli presented were analyzed online in order to determine the neuron's preferred orientation, RF size, SF and TF. All stimuli were presented for 8-12 repetitions.

Orientation Tuning

The neurons preferred orientation tuning was determined with square-wave gratings of 8 orientations, with 22.5° spacing. Each run of the stimulus was 5.5s long: the grating was stationary for 0.5s, then drifted in one direction for 2s, then paused for 0.5s, then drifted in the opposite direction for 2s, then pausing for a final 0.5s, with 0.5s of

grey mean luminance between presentations. The preferred direction was taken as the angle that elicited the highest spike rate.

Receptive Field Size

Preferred stimulus size was determined with a circular aperture containing a sine-wave grating, as well as a full field grating with a circular aperture of grey in the center. Both stimuli were 3s long: a stationary grating appeared for 0.5s then drifted for 2s, then paused for a final 0.5s. Six different stimulus diameters were presented randomly, 64°, 48°, 32°, 24°, 12° and 8°, with 0.5s of grey mean luminance between each repetition. These two stimuli allowed the size tuning of the neuron to be tested, in addition to confirming that the monitor was positioned in the center of the neuron's receptive field. The stimulus size used on subsequent tests was chosen as either the diameter where the size tuning function began to asymptote in neurons lacking surround suppression (SS), or the peak of the function for neurons with SS.

Spatiotemporal Tuning

Neurons' preferred spatial and temporal frequencies were determined with sine-wave gratings which drifted in the preferred direction and were the preferred RF size. We presented 36 different combinations of SFs (0.01, 0.02, 0.04, 0.08, 0.16, 0.32 cycles per degree (cpd)) and TFs (0.25, 0.50, 1, 2, 4, 8Hz). Each stimulus presentation lasted for 3s: each grating appeared and remained stationary for 0.5s, then drifted for 2s, then paused for another 0.5s. A grey mean luminance was presented for 0.5s between each combination. The preferred SF and TF were chosen based on an online tuning curve.

Top-Up Contrast Adaptation

The top-up contrast adaptation protocol was used due to the ease of comparison to previous mouse experiments, and was originally used in cats and primates (Movshon and Lennie, 1979; Duong and Freeman, 2007; Dhruv et al., 2011; LeDue et al., 2013). Sine-wave contrast is defined as:

$$\text{Michelson Contrast} = \frac{\text{Luminance}_{\text{max}} - \text{Luminance}_{\text{min}}}{\text{Luminance}_{\text{max}} + \text{Luminance}_{\text{min}}} \quad (4)$$

where $\text{Luminance}_{\text{max}}$ and $\text{Luminance}_{\text{min}}$ are the maximum and minimum luminance, respectively. All contrast stimuli were presented at the neuron's preferred orientation, RF size, and TF. Non-adapted contrast response functions were obtained by recording responses to ten contrasts (0.04, 0.08, 0.12, 0.16, 0.24, 0.32, 0.48, 0.64, 0.82, 1) in random order for 0.5s tests, with 4s of mean luminance between stimuli. Adaptation blocks consisted of 60s of moving sine-wave grating at 0.2-0.32 contrast, followed by 8-12 repetitions of 0.5s tests (aforementioned contrasts), with 4s of top-up between each presented contrast. Adapted contrast response functions were obtained in two blocks: 1) the adapting grating and the testing grating were composed of identical SFs, which will be referred to as "matched adaptation"; and 2) the adapting and test gratings were composed of two different SFs that were carefully selected as to elicit the same spike rate from the neuron being recorded from. This condition will be referred to as "unmatched adaptation".

3.2.4 *Data Analysis*

Spikes were sorted offline using Spike2 software, which used a template-matching algorithm to identify and sort spikes, and then displayed potential spikes with a

principle components analysis. Data were then analyzed in MATLAB, where neuronal responses were represented as spike density functions (SDF) with 1 kHz resolution generated by convolving a delta function at each spike arrival time with a Gaussian window. For each neuron, the magnitude of orientation, size, and spatiotemporal tuning was quantified using a DI (eqn. 2, DeAngelis and Uka, 2003).

Curve Fitting

Contrast response functions were fit using the least squares method. Sigmoid curves were fit to the mean responses from top-up contrast response functions (Albrecht and Hamilton, 1982):

$$R(c_i) = \frac{R_{max} * c_i n}{c_i n + c_{50} n} + M \quad (5)$$

where $R(c_i)$ is the amplitude of the evoked response at contrast c_i , M is the spontaneous rate, n is the exponent that determines the steepness of the curve, R_{max} is the maximum elevation in response above the spontaneous rate, and c_{50} is the contrast that generates a response elevation of half R_{max}.

We also calculated the area under the contrast response functions by determining the difference over sum for area under the log contrast curve. This was an added measure to quantify the magnitude of adaptation, and to compare the differences between the matched and unmatched adaptation conditions. The upper limits of the contrast response functions were adjusted for those functions that did not saturate at high contrasts. This was done to ensure accurate R_{max} and areas were determined, and not erroneous extrapolated values.

The last analysis we performed quantified the number phase sensitive neurons in our sample by utilizing the F_1/F_0 ratio. The F_1/F_0 ratio is calculated by dividing the first Fourier coefficient of the response (F_1) by the mean time-averaged response (F_0). A value >1 means that the neuron is sensitive to the phase of the stimulus.

For statistical comparisons Wilcoxon sign rank tests were performed for repeated measures, and rank sum tests for comparison between groups. Bonferroni corrections were applied to account for multiple comparisons.

3.3 Results

Contrast adaptation was measured in 67 visually responsive cells in V1 of 14 C57BL/6 J mice. There were 51 cells that had an orientation tuning DI >0.425, suggesting that the activity of these neurons were substantially modulated by the orientation of the stimulus grating. The units' preferred SFs ranged from 0.01 to 0.04cpd and preferred TFs ranged from 0.25 to 8 Hz. Of the 67 cells, 60 were not phase-sensitive based on the F_1/F_0 ratio.

3.3.1 Top-Up Adaptation

A top-up contrast adaptation protocol, used previously in mice and originating in studies of cats and primates, was used to quantify differences in the magnitude of adaptation after prolonged presentation of gratings in the two adaptation conditions: matched and unmatched adaptation.

Figures 5A, B, C and D are four example cells showing the three contrast response functions calculated for each unit: blue is the non-adapted function, green is the contrast response function after unmatched adaptation, and red is the function after

matched adaptation. Figures 5A and B show two cells that adapted more after matched adaptation, and are representative of the majority of our sample. Figure 5C shows a cell that adapted the same amount in both conditions, and figure 5D shows a neuron that adapted more after unmatched adaptation.

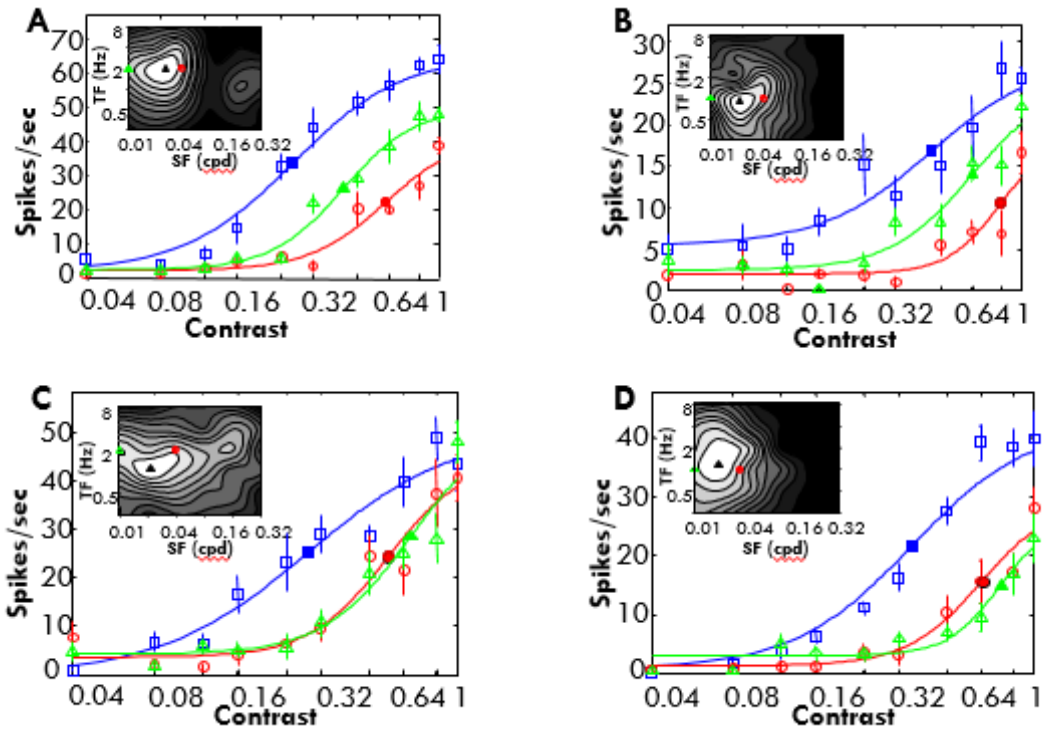

Figure 5: Example contrast response functions. Contrast values are referenced on the abscissa and the neurons' responses in spikes/second are on the ordinate. The blue sigmoid curves with square data points represent the neurons' responses after no adaptation, the red curve with circle data points represent responses after matched adaptation, and the green curves with triangle data points are responses after unmatched adaptation. The insets are spatiotemporal contour plots, with the TF on the x-axis and SF on the y-axis. The black triangle represents the neuron's preferred combination of SF and TF, the red circle indicates the SF used for all test gratings, and during matched adaptation, and the green triangle indicates the SF used during unmatched adaptation. A and B are two neurons which adapted more after matched adaptation, C is a neuron which adapted the same in both conditions, and D is a neuron which adapted more after unmatched.

Sigmoid fits to each contrast response function are shown as thin lines in figure 5,

and the c_{50} and R_{max} parameters extracted from these fits were used to quantitatively analyze changes following top-up adaptation. Figures 6A, C, and E compare c_{50} values between conditions, and figures 6B, D, and F compare R_{max} values via a difference over sum calculation. Figures 6A and C show histograms that compare non-adapted c_{50} values to c_{50} values after adaptation when the SF of the adaptor either matched or differed from the test gratings, respectively. For both conditions, c_{50} values were significantly higher following adaptation (63/66 matched adaptation, mean change 19.5%; 62/66 for unmatched adaptation, mean change 12.5%; $p < 0.0001$ for both). Figure 6E shows a histogram comparing the c_{50} values from matched and unmatched adaptation, with positive numbers indicating a rightward curve shift. c_{50} values were significantly higher after matched adaptation (44/66, mean change 6.9%; $p<0.0001$).

Figures 6B and D show histograms which compare non-adapted R_{max} values to R_{max} values from curves adapted and tested with the same SF and curves adapted at a different SF, respectively. For both conditions, R_{max} values were significantly lower in the adapted condition (matched adaptation SF: 59/66, mean change 9.2%; unmatched adaptation: 62/66, mean change 10.1%; $p<0.00001$ for both). Figure 6F shows a histogram comparing R_{max} values from the two adaptation conditions. We found that there was no significant difference in R_{max} values when comparing matched and unmatched adaptation (30/66 cells had larger R_{max} values from curves obtained after unmatched adaptation, mean change 8.8%, $p > 0.2$).

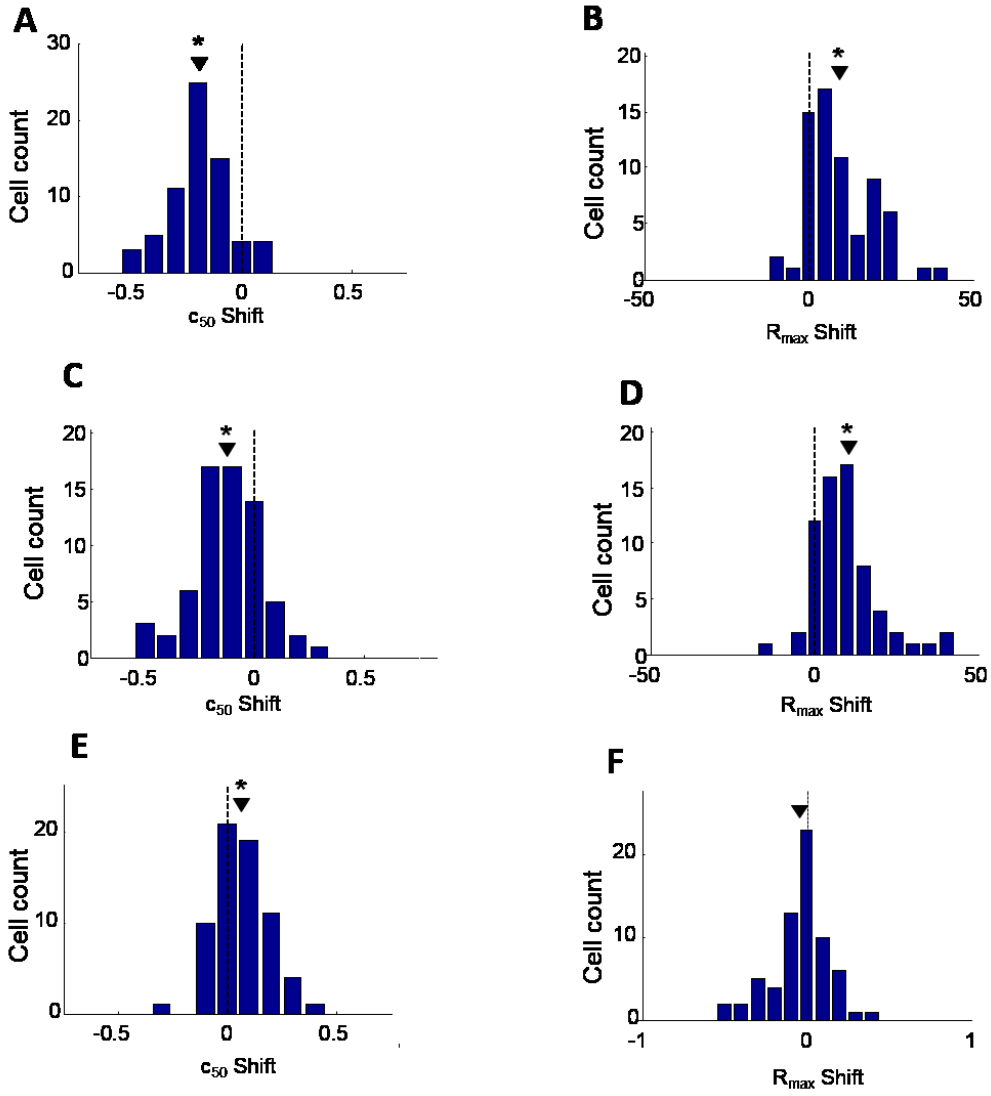

Figure 6: Difference over sum changes in c_{50} and R_{max}. For all histograms negative values indicate a decrease in value, positive numbers indicate an increase in value, and inverted triangles represent the mean change. A and C are histograms showing the difference in c_{50} values between non-adapted and matched and unmatched adaptation, respectively. E shows a histogram displaying the difference in c_{50} values from matched and unmatched adaptation. B and D are histograms showing the different in R_{max} values between non-adapted and matched and unmatched adaptation, respectively. F shows a histogram displaying the shift in R_{max} values from matched and unmatched adaptation.

Figures 7A-C show histograms comparing the difference over sum for area under

the log contrast curve. Figures 7A and B compare the area under non-adapted curves to matched and unmatched adaptation curves, respectively. For both conditions, the area is greater under the non-adapted curve (mean changes were -26.7% and -23.4% for neurons adapted with the same SF and different SF, respectively; $p < 0.0001$ for both). Figure 7C is comparing the area under the curve for the two adaptation conditions, with the area being significantly smaller under the curve after matched adaptation (mean change = 3.6%, $p < 0.05$).

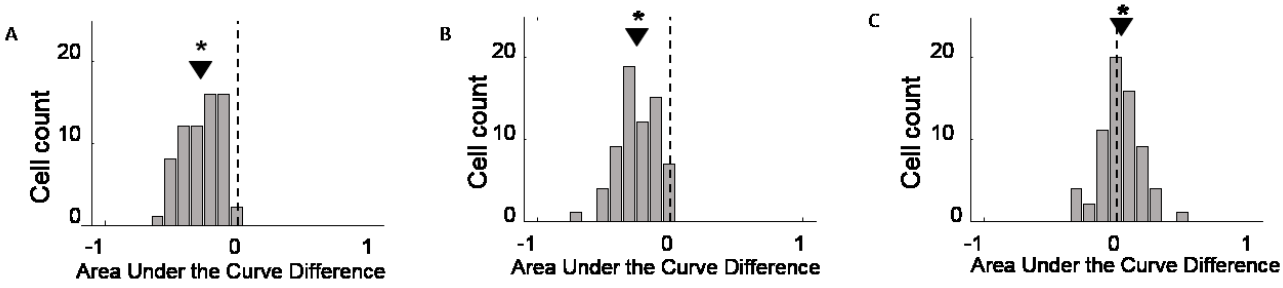

Figure 7: Difference over sum for area under the log contrast curve. For all plots inverted triangles indicate the mean difference. A and B show histograms comparing the difference over sum for area under the log contrast curve for non-adapted curves and matched and unmatched adapted curves, respectively. Negative values indicate more area under the non-adapted curve. C shows a histogram comparing the area under the curve between curves obtained after matched or unmatched adaptation. Negative values indicate more area under the matched adapted curve.

3.4 Discussion

The current study examined pattern-selective contrast adaptation in mouse V1 by utilizing a top-up adaptation protocol that originated in cats, but has been adapted for use in mice. We built on a previous study from our lab (LeDue et al., 2013) that demonstrated contrast adaptation in mouse V1 is specific in the spatiotemporal domain, but failed to control for spike rate. To address this, we performed identical experiments but more carefully selected our SFs to ensure that they elicited the same spike rate from neurons,

and adapted neurons in two conditions: matched and unmatched adaptation. We found that matched adaptation caused neurons to adapt more than after unmatched adaptation, which supports what LeDue et al. (2013) previously reported.

There are multiple previously published papers which have used similar top-up adaptation protocols to investigate contrast adpation (e.g., Movshon and Lennie, 1979; Duong and Freeman, 2007; Dhruv et al., 2011), and are therefore comparable to the data presented here. Our current adaptation protocol is designed after Movshon and Lennie's (1979) experimental protocol where they studied SF specificity of contrast adaptation in cat V1 and had conditions similar to our matched and unmatched adaptation. Our findings in mouse V1 are similar to their findings as both studies observed greater adaptation when the adapting and test gratings were identical, suggesting that contrast adaptation is pattern-specific. The current study extends this finding into a genetically tractable animal model where there exists an expanded toolbox to investigate the mechanisms underlying this specificity.

One of the current global goals of mouse vision research is to determine whether results obtained from the mouse visual system are generalizable to other species, which is accomplished by performing fundamental vision experiments in mice and comparing the results to those previously obtained in cats and primates. By showing that mice do exhibit pattern-specific contrast adaptation, the current study has shown that mouse visual systems respond comparably to higher order mammals. The need for these fundamental baseline experiments is important because the genetic tools available in mice allow perturbation of the system with temporal and spatial accuracy unavailable in higher order mammals or by using pharmacological tools. Future experiments utilizing transgenic

mice should target inhibitory interneuron populations which would allow the contribution of excitatory and inhibitory inputs to be parsed, and would allow for a causal link to be made between cell type and physiological manifestation. Determining the specific circuitry in mice also provides a strong foundation for future experiments in higher order mammals as researchers will better understand the neural networks on a smaller and simpler scale, providing more informed starting places for new research projects.

CHAPTER 4: CONCLUSIONS

Mouse vision research is a relatively new field, with many fundamental experiments still lacking in the quickly-growing body of literature. This thesis includes two such studies, with the first project examining and quantifying orientation adaptation in mouse V1, and the second examining whether the magnitude of contrast adaptation in mouse V1 is spike rate dependent. For the orientation adaptation study, we demonstrated that after adaptation orientation tuning curves in mouse V1 shift similarly to those in more traditional models (cats: Dragoi et al., 2001; primates: Patterson et al., 2013). In the contrast adaptation study we demonstrated that, as previously shown in cats in cat V1 (Movshon and Lennie, 1979), contrast adaptation in mouse V1 is pattern-specific. This finding also corroborates the findings from LeDue et al. (2013) who showed that contrast adaptation in mouse V1 is specific on the spatiotemporal domain.

Future Directions

The primary motivation behind using the non-visual mouse in vision research is the genetic tools readily available in this species. Optogenetics and fluorescent markers allow researchers to perturb mouse neural networks both spatially and temporally (Runyan et al. 2010; Cai et al. 2013) with an accuracy that is unattainable pharmacologically, and with genetics that are not yet readily available in higher-order mammals. Using mice for foundational work uncovering the neural networks behind cortical plasticity and neural adaptation provides an optimal starting point for this area of research as their visual systems are simpler than those of cats and primates, yet are similar enough that the findings are relevant. Future directions in the field of mouse vision will aim at uncovering specific networks involved at various stages of processing,

as well as attempting to correlate said neural networks with perception and the resulting behaviour.

WORKS CITED

Abbonizio G, Langley K, Clifford CWG (2002) Contrast adaptation may enhance contrast discrimination. Spat Vis 16:45–58.

Adesnik H, Bruns W, Taniguchi H, Huang ZJ, Scanziani M (2012) A neural circuit for spatial summation in visual cortex. Nature 490:226–231.

Andermann ML, Kerlin AM, Roumis DK, Glickfeld LL, Reid RC (2011) Functional specialization of mouse higher visual cortical areas. Neuron 72:1025–1039.

Bachatene L, Bharmauria V, Rouat J, Molotchnikoff S (2012) Adaptation-induced plasticity and spike waveforms in cat visual cortex. Neuroreport 23:88–92.

Bair W, Movshon JA (2004) Adaptive temporal integration of motion in direction-selective neurons in macaque visual cortex. J Neurosci 24:7305–7323.

Baker M (2013) Through the eyes of a mouse. Nature 502:156–158.

Balkema GW, Mangini NJ, Pinto LH, Vanable JW (1984) Visually evoked eye movements in mouse mutants and inbred strains. A screening report. Invest Ophthalmol Vis Sci 25:795–800.

Blakemore C, Campbell F (1969) Adaptation to spatial stimuli. J Physiol 200:11–13.

Bonds AB (1991) Temporal dynamics of contrast gain in single cells of the cat striate cortex. Vis Neurosci 6:239–255.

Bonhoeffer T, Grinvald A (1991) Iso-orientation domains in cat visual cortex are arranged in pinwheel-like patterns. Nature 353:429–431.

Brainard DH (1997) The psychophysics toolbox. Spat Vis 10:433–436.

Busse L, Ayaz A, Dhruv NT, Katzner S, Saleem AB, Schölvinck ML, Zaharia AD, Carandini M (2011) The detection of visual contrast in the behaving mouse. J Neurosci 31:11351–11361.

Bussey T, Saksida L, Rothblat L (2001) Discrimination of computer-graphic stimuli by mice: a method for the behavioral characterization of transgenic and gene-knockout models. Behav Neurosci 4:957–960.

Cai D, Cohen KB, Luo T, Lichtman JW, Sanes JR (2013) Improved tools for the Brainbow toolbox. Nat Methods 10:540–547.

Callaway EM (1998) Local circuits in primary visual cortex of the macaque monkey. Annu Rev Neurosci 21:47–74.

Carandini M (2000) Visual cortex: Fatigue and adaptation. Curr Biol CB 10:R605–R607.

Carandini M, Demb JB, Mante V, Tolhurst DJ, Dan Y, Olshausen B a, Gallant JL, Rust NC (2005) Do we know what the early visual system does? J Neurosci 25:10577–10597.

Carandini M, Movshon J a, Ferster D (1998) Pattern adaptation and cross-orientation interactions in the primary visual cortex. Neuropharmacology 37:501–511.

Cattan S, Bachatene L, Bharmauria V, Jeyabalaratnam J, Milleret C, Molotchnikoff S (2014) Comparative analysis of orientation maps in areas 17 and 18 of the cat primary visual cortex following adaptation. Eur J Neurosci 40:2554–2563.

Clifford CWG (2002) Perceptual adaptation: motion parallels orientation. Trends Cogn Sci 6:136–143.

Das a, Gilbert CD (1999) Topography of contextual modulations mediated by short-range interactions in primary visual cortex. Nature 399:655–661.

De Valois RL, Albrecht DG, Thorell LG (1982) Spatial frequency selectivity of cells in macaque visual cortex. Vision Res 22:545–559.

DeAngelis GC, Ohzawa I, Freeman RD (1993) Spatiotemporal organization of simple-cell receptive fields in the cat's striate cortex. II. Linearity of temporal and spatial summation. J Neurophysiol 69:1118–1135.

DeAngelis GC, Uka T (2003) Coding of horizontal disparity and velocity by MT neurons in the alert macaque. J Neurophysiol 89:1094–1111.

Dhruv NT, Tailby C, Sokol SH, Lennie P (2011) Multiple adaptable mechanisms early in the primate visual pathway. J Neurosci 31:15016–15025.

Dräger UC (1975a) Receptive fields of single cells and topography in mouse visual cortex. J Comp Neurol 160:269–290.

Dräger UC (1975b) Receptive fields fo single cells and topography in mouse visual cortex. J Comp Neurol 60:269–290.

Dräger UC, Olsen JF (1980) Origins of crossed and uncrossed retinal projections in pigmented and albino mice. J Comp Neurol 191:383–412.

Dragoi V, Rivadulla C, Sur M (2001) Foci of orientation plasticity in visual cortex. Nature 411:80–86.

Dragoi V, Sharma J, Sur M (2000) Adaptation-induced plasticity of orientation tuning in adult visual cortex. Neuron 28:287–298.

Duong T, Freeman RD (2007) Spatial frequency-specific contrast adaptation originates in the primary visual cortex. J Neurophysiol 98:187–195.

Enroth-Cugell C, Robson JG (1984) Functional characteristics and diversity of cat retinal ganglion cells. Basic characteristics and quantitative description. Invest Ophthalmol Vis Sci 25:250–267.

Foley JM, Chen CC (1997) Analysis of the effect of pattern adaptation on pattern pedestal effects: a two-process model. Vision Res 37:2779–2788.

Foster K, Gaska J, Nagler M, Pollen DA (1985) Spatial and temporal frequency selectivity of neurones in visual cortical areas V1 and V2 of the macaque monkey. J Physiol 365:331–363.

Fuchs AF, Kaneko CR, Scudder CA (1985) Brainstem control of saccadic eye movements. Annu Rev Neurosci 8:307–337.

Gao E, DeAngelis GC, Burkhalter A (2010) Parallel input channels to mouse primary visual cortex. J Neurosci 30:5912–5926.

Ghisovan N, Nemri A, Shumikhina S, Molotchnikoff S (2009) Long adaptation reveals mostly attractive shifts of orientation tuning in cat primary visual cortex. Neuroscience 164:1274–1283.

Gibson J, Radner M (1937) Adaptation, after-effect and contrast in the perception of tilted lines. J Exp Psychol 12:453–467.

Greenlee M, Heitger F (1988) The functional role of contrast adaptation. Vision Res 28:791–797.

Hawken MJ, Shapley RM, Grosof DH (1996) Temporal-frequency selectivity in monkey visual cortex. Vis Neurosci 13:477–492.

Hubel D, Wiesel T (1959) Receptive fields of single neurones in the cat's striate cortex. J Physiol 148:574–591.

Hubel DH, Wiesel TN (1963) Shape and arrangement of columns in cat's striate cortex. J Physiol 165:559–568.

Hubel DH, Wiesel TN (1968) Receptive fields and functional architecture of monkey striate cortex. J Physiol 195:215–243.

Hubel DH, Wiesel TN (1974) Uniformity of monkey striate cortex: a parallel relationship between field size, scatter, and magnification factor. J Comp Neurol 158:295–305.

Huberman AD, Niell CM (2011) What can mice tell us about how vision works? Trends Neurosci 34:464–473.

Ibbotson MR (2005) Contrast and temporal frequency-related adaptation in the pretectal nucleus of the optic tract. J Neurophysiol 94:136–146.

Irvin GE, Casagrande VA, Norton TT (1993) Center/surround relationships of magnocellular, parvocellular, and koniocellular relay cells in primate lateral geniculate nucleus. Vis Neurosci 10:363–373.

Jeon CJ, Strettoi E, Masland RH (1998) The major cell populations of the mouse retina. J Neurosci 18:8936–8946.

Kalatsky V a, Stryker MP (2003) New paradigm for optical imaging: temporally encoded maps of intrinsic signal. Neuron 38:529–545.

Kohn A (2007) Visual adaptation: physiology, mechanisms, and functional benefits. J Neurophysiol 97:3155–3164.

Kohn A, Movshon JA (2004) Adaptation changes the direction tuning of macaque MT neurons. Nat Neurosci 7:764–772.

Kuhlmann L, Vidyasagar TR (2011) A computational study of how orientation bias in the lateral geniculate nucleus can give rise to orientation selectivity in primary visual cortex. Front Syst Neurosci 5:81.

LeDue EE, King JL, Stover KR, Crowder NA (2013) Spatiotemporal specificity of contrast adaptation in mouse primary visual cortex. Front Neural Circuits 7:154.

Levinson E, Sekuler R (1976) Adaptation alters perceived direction of motion. Vision Res 16:779–781.

Levy M, Lu Z, Dion G, Kara P (2014) The Shape of Dendritic Arbors in Different Functional Domains of the Cortical Orientation Map. J Neurosci 34:3231–3236.

Lien AD, Scanziani M (2013) Tuned thalamic excitation is amplified by visual cortical circuits. Nat Neurosci 16:1315–1323.

Malach R, Amir Y, Harel M, Grinvald a (1993) Relationship between intrinsic connections and functional architecture revealed by optical imaging and in vivo targeted biocytin injections in primate striate cortex. Proc Natl Acad Sci U S A 90:10469–10473.

Maldonado PE (1997) Orientation Selectivity in Pinwheel Centers in Cat Striate Cortex. Science (80-) 276:1551–1555.

Mangini NJ, Pearlman AL (1980) Laminar distribution of receptive field properties in the primary visual cortex of the mouse. J Comp Neurol 193:203–222.

Marshel JH, Garrett ME, Nauhaus I, Callaway EM (2011) Functional specialization of seven mouse visual cortical areas. Neuron 72:1040–1054.

Movshon BYJA, Thompson ID, Tolhurst DJ (1978) Spatial and temporal contrast sensitivity of neurones in areas 17 and 18 of the cat's visual cortex. J Physiol 283:101–120.

Movshon JA, Lennie P (1979) Pattern-selective adaptation in visual cortical neurones. Nature 278:850–852.

Nauhaus I, Benucci A, Carandini M, Ringach DL (2008) Neuronal selectivity and local map structure in visual cortex. Neuron 57:673–679.

Niell CM, Stryker MP (2008) Highly selective receptive fields in mouse visual cortex. J Neurosci 28:7520–7536.

Nowak LG, Barone P (2009) Contrast adaptation contributes to contrast-invariance of orientation tuning of primate V1 cells. PLoS One 4:e4781.

Ohki K, Chung S, Ch'ng YH, Kara P, Reid RC (2005) Functional imaging with cellular resolution reveals precise micro-architecture in visual cortex. Nature 433:597–603.

Ohzawa I, Sclar G, Freeman RD (1982) Contrast gain control in the cat visual cortex. Nature 298:266–268.

Ohzawa I, Sclar G, Freeman RD (1985) Contrast gain control in the cat's visual system. J Neurophysiol 54:651–667.

Packer O, Hendrickson AE, Curcio CA (1989) Photoreceptor topography of the retina in the adult pigtail macaque (Macaca nemestrina). J Comp Neurol 288:165–183.

Patterson C a, Duijnhouwer J, Wissig SC, Krekelberg B, Kohn A (2014) Similar adaptation effects in primary visual cortex and area MT of the macaque monkey under matched stimulus conditions. J Neurophysiol 111:1203–1213.

Patterson CA, Wissig SC, Kohn A (2013) Distinct effects of brief and prolonged adaptation on orientation tuning in primary visual cortex. J Neurosci 33:532–543.

Patterson R, Becker S (1996) Direction-selective adaptation and simultaneous contrast induced by stereoscopic (cyclopean) motion. Vision Res 36:1773–1781.

Paxinos G, Franklin K (2001) The Mouse Brain in Stereotaxic Coordinates, Second. San Diego: Academic Press.

Pelli D (1997) The videotookbox software for visual psychophysics: transforming numbers into movies. Spat Vis 10:437–447.

Porciatti V, Pizzorusso T, Maffei L (1999) The visual physiology of the wild type mouse determined with pattern VEPs. Vision Res 39:3071–3081.

Priebe NJ, Lampl I, Ferster D (2010) Mechanisms of direction selectivity in cat primary visual cortex as revealed by visual adaptation. J Neurophysiol 104:2615–2623.

Prusky GT, Alam NM, Beekman S, Douglas RM (2004) Rapid quantification of adult and developing mouse spatial vision using a virtual optomotor system. Invest Ophthalmol Vis Sci 45:4611–4616.

Prusky GT, West PW, Douglas RM (2000) Behavioral assessment of visual acuity in mice and rats. Vision Res 40:2201–2209.

Reid RC, Alonso JM (1995) Specificity of monosynaptic connections from thalamus to visual cortex. Nature 378:281–284.

Rodieck RW, Watanabe M (1993) Survey of the morphology of macaque retinal ganglion cells that project to the pretectum, superior colliculus, and parvicellular laminae of the lateral geniculate nucleus. J Comp Neurol 338:289–303.

Runyan C a, Schummers J, Van Wart A, Kuhlman SJ, Wilson NR, Huang ZJ, Sur M (2010) Response features of parvalbumin-expressing interneurons suggest precise roles for subtypes of inhibition in visual cortex. Neuron 67:847–857.

Schall JD, Hanes DP, Thompson KG, King DJ (1995) Saccade target selection in frontal eye field of macaque. I. Visual and premovement activation. J Neurosci 15:6905–6918.

Schiller PH, Finlay BL, Volman SF (1976) Quantitative studies of single-cell properties in monkey striate cortex. II. Orientation specificity and ocular dominance. J Neurophysiol 39:1320–1333.

Scholl B, Tan AYY, Corey J, Priebe NJ (2013) Emergence of orientation selectivity in the Mammalian visual pathway. J Neurosci 33:10616–10624.

Schrater PR, Simoncelli EP (1998) Local velocity representation: evidence from motion adaptation. Vision Res 38:3899–3912.

Schuett S, Bonhoeffer T, Hübener M (2002) Mapping retinotopic structure in mouse visual cortex with optical imaging. J Neurosci 22:6549–6559.

Schwartz O, Sejnowski TJ, Dayan P (2009) Perceptual organization in the tilt illusion. J Vis 9:19.1–20.

Sclar G, Lennie P, DePriest DD (1989) Contrast adaptation in striate cortex of macaque. Vision Res 29:747–755.

Skottun BC, De Valois RL, Grosof DH, Movshon JA, Albrecht DG, Bonds AB (1991) Classifying simple and complex cells on the basis of response modulation. Vision Res 31:1079–1086.

Smith E, Chino Y, Ridder W, Kitagawa K, Langson A (1990) Orientation bias of neurons in the lateral geniculate nucleus of macaque monkeys. Vis Neurosci 5:525–545.

Stroud AC, Ledue EE, Crowder NA (2012) Orientation specificity of contrast adaptation in mouse primary visual cortex. J Neurophysiol 108:1381–1391.

Swindale N V (1998) Orientation tuning curves : empirical description and estimation of parameters. Biol Cybern 78:45–56.

Vaiceliunaite A, Erisken S, Franzen F, Katzner S, Busse L (2013) Spatial integration in mouse primary visual cortex. J Neurophysiol 110:964–972.

Van den Bergh G, Zhang B, Arckens L, Chino YM (2010) Receptive-field properties of V1 and V2 neurons in mice and macaque monkeys. J Comp Neurol 518:2051–2070.

Van Hooser SD, Heimel JAF, Chung S, Nelson SB, Toth LJ (2005) Orientation selectivity without orientation maps in visual cortex of a highly visual mammal. J Neurosci 25:19–28.

Wang Q, Burkhalter A (2007) Area Map of Mouse Visual Cortex. J Comp Neurol 357:339–357.

Wielaard DJ, Shelley M, McLaughlin D, Shapley R (2001) How simple cells are made in a nonlinear network model of the visual cortex. J Neurosci 21:5203–5211.

Wikler K, Rakic P (1990) Distribution of Photoreceptor Nocturnal Primates Subtypes in the Retina of Diurnal and Nocturnal Primates. J Neurosci 10:3390–3401.

Wimbauer S, Wenisch OG, Miller KD, van Hemmen JL (1997) Development of spatiotemporal receptive fields of simple cells: I. Model formulation. Biol Cybern 77:453–461.

Wissig SC, Kohn A (2012) The influence of surround suppression on adaptation effects in primary visual cortex. J Neurophysiol 107:3370–3384.

Wong A, Brown R (2006) Visual detection, pattern discrimination and visual acuity in 14 strains of mice. Genes Brain Behav 5:389–403.

Xu X, Ichida J, Shostak Y, Bonds A, Casagrande VA (2002) Are primate lateral geniculate nucleus (LGN) cells really sensitive to orientation or direction? Vis Neurosci 19:97–108.